SRRT promotes prostate cancer progression and serves as a prognostic biomarker through STAT3 pathway activation

LINGXIANG LU[1*], KE WU[2*], ZHENFAN WANG[1], RUOXI YANG[3], KAI LI[2], SHUAI GUO[1], FEI WANG[2] and ZHENG MA[1]

[1]Department of Urology, Suzhou Ninth People's Hospital, Soochow University, Suzhou, Jiangsu 215000, P.R. China; [2]Department of Urology, The Affiliated Suzhou Hospital of Nanjing Medical University, Suzhou Municipal Hospital, Gusu School, Nanjing Medical University, Suzhou, Jiangsu 215000, P.R. China; [3]School of Medicine, Tongji University, Shanghai 200000, P.R. China

Received March 10, 2026; Accepted April 23, 2026

DOI: 10.3892/or.2026.9134

Abstract. Prostate cancer (PC) is a highly prevalent malignancy in men with substantial prognostic heterogeneity. The present study aimed to identify novel prognostic biomarkers and investigate their functional roles and underlying mechanisms in PC. To this end, integrated bioinformatics analyses were performed using The Cancer Genome Atlas-prostate adenocarcinoma cohort and two Gene Expression Omnibus datasets. A total of 95 common differentially expressed genes were identified and were significantly enriched in the STAT3 signaling pathway. Lasso and Cox regression analyses screened nine independent prognostic genes, among which SRRT exhibited the highest risk coefficient. The constructed risk model showed strong predictive performance for disease-free survival and favorable calibration in nomogram analysis. Experimental validation demonstrated that SRRT was markedly upregulated in PC tissues and cell lines, and functional assays revealed that SRRT knockdown inhibited, whereas overexpression promoted, proliferation and migration of DU145 and PC-3 cells *in vitro* and tumor growth *in vivo*. Mechanistically, SRRT enhanced STAT3 phosphorylation, and activation of STAT3 by colivelin partially reversed the suppressive effects of SRRT silencing, indicating that SRRT promotes PC progression through activation of the STAT3 signaling pathway. Collectively, SRRT acts as an independent adverse prognostic biomarker that promotes PC progression, and the present findings provide integrated bioinformatic and experimental evidence linking SRRT to STAT3 pathway activation.

Correspondence to: Dr Zheng Ma, Department of Urology, Suzhou Ninth People's Hospital, Soochow University, 2666 Ludang Road, Taihu New City, Wujiang, Suzhou, Jiangsu 215000, P.R. China
E-mail: mazheng851230@yeah.net

Dr Fei Wang, Department of Urology, The Affiliated Suzhou Hospital of Nanjing Medical University, Suzhou Municipal Hospital, Gusu School, Nanjing Medical University, 26 Daoqian Road, Suzhou, Jiangsu 215000, P.R. China
E-mail: feiwang202207@163.com

*Contributed equally

Key words: prostate adenocarcinoma, SRRT, STAT3 signaling pathway, biomarker

Introduction

Prostate cancer (PC) is one of the malignant tumors with a high incidence among men worldwide and has become a major public health issue threatening men's reproductive health and overall survival (1,2). In recent years, although diagnostic and therapeutic approaches such as prostate-specific antigen screening, radical prostatectomy, radiotherapy and androgen deprivation therapy have been continuously developed, significantly improving the prognosis of some patients, the clinical outcomes of patients with advanced or metastatic PC remain unsatisfactory (3,4). Tumor recurrence, drug resistance and metastasis are still major challenges in clinical treatment (5). Currently used clinical prognostic evaluation indicators have limitations: They cannot accurately distinguish survival differences among patients with different risk stratifications, nor can they provide a sufficient molecular-level basis for the formulation of individualized treatment regimens (6). Recent studies have attempted to improve prognostic stratification by integrating gene expression signatures. Xie *et al* (7) constructed a prognostic model based on ribosome biogenesis-related genes, highlighting the value of molecular features in risk prediction. However, the heterogeneity of PC indicates that additional robust biomarkers and regulatory mechanisms remain to be identified. Therefore, exploring key molecular biomarkers closely related to the occurrence, development and prognosis of PC, and clarifying their regulatory mechanisms, is of great significance for optimizing the PC prognostic evaluation system and developing novel molecular stratification strategies and improving risk-adapted clinical management.

With the rapid development of high-throughput sequencing technology and bioinformatics, public databases [for example, The Cancer Genome Atlas (TCGA); Gene Expression Omnibus, (GEO)] have accumulated a large amount of PC gene expression and clinical prognostic data, providing strong support for the systematic screening of differentially expressed

genes (DEGs) and prognosis-related molecular targets (8,9). Integrative analysis of multiple datasets can effectively reduce the bias of a single dataset and improve the reliability of screening results. Functional enrichment analysis of DEGs can further reveal the key biological processes and signaling pathways they participate in, pointing out directions for subsequent mechanistic studies (10). Existing studies have shown that the abnormal activation of multiple signaling pathways plays a core role in the malignant progression of PC. Among them, the sustained activation of the Signal Transducer and Activator of Transcription 3 (STAT3) signaling pathway can promote the occurrence, development, and metastasis of PC by regulating the expression of genes related to cell proliferation, apoptosis and migration, highlighting its important role in PC progression and its potential relevance for therapeutic research (11,12).

SRRT, a serine/arginine-rich splicing factor, was initially found to be involved in the regulation of RNA splicing (13,14). In recent years, studies have suggested that it is abnormally expressed in a variety of malignant tumors and is closely related to tumor cell proliferation, migration and prognosis (15). For example, SRRT is highly expressed in liver cancer (16) and breast cancer (17), and its high expression is significantly associated with poor prognosis of patients, which can promote tumor progression by regulating downstream signaling pathways (18). Notably, it has been also previously reported that SRRT is associated with prostate cancer (PC) progression and poor prognosis (14). However, the precise functional role and underlying molecular mechanisms of SRRT in PC remain incompletely understood, which needs further investigation.

Based on this, the present study first integrated the TCGA-PRAD dataset and the GSE32571, GSE3325 datasets in the GEO database to screen common DEGs in PC tumor and adjacent normal tissues and analyzed their functional characteristics by combining Gene Ontology (GO)/Kyoto Encyclopedia of Genes and Genomes (KEGG) enrichment analyses. Subsequently, Lasso regression and Cox regression analyses were used to screen independent prognostic genes, construct a prognostic risk model, and verify its efficacy. Finally, focusing on the SRRT gene with the highest risk coefficient, *in vitro* cell experiments [Cell Counting Kit-8 (CCK-8), Transwell, scratch assay and western blotting) were conducted to verify its effects on the proliferation, and migration of PC cells, and explore its regulatory relationship with the STAT3 signaling pathway. The present study aims to further elucidate the functional role and molecular mechanism of SRRT in PC, with a particular focus on its potential involvement in STAT3 signaling.

Materials and methods

Data acquisition and preprocessing. Gene expression data of PC tumors and adjacent normal tissues were obtained from the TCGA-PRAD dataset and the GSE32571 and GSE3325 datasets in the GEO database. The TCGA-PRAD cohort included 502 primary tumor samples and 52 normal prostate tissues with available clinical and survival information. The GSE32571 dataset comprised 59 PC samples and 39 normal prostate samples. The GSE3325 dataset included 13 PC samples and 6 normal prostate samples. TCGA-PRAD RNA-sequencing (RNA-seq) data were downloaded from the Genomic Data Commons portal in HTSeq-count format. The GSE32571 and GSE3325 datasets were obtained as raw CEL files or series matrix files using the GEOquery R package (Bioconductor; version 2.78; https://bioconductor.org/packages/release/bioc/html/GEOquery.html). For TCGA RNA-seq data, raw count data were used for downstream analysis.

Screening of DEGs. Differential expression analysis was performed using methods appropriate for each data type. For RNA-seq data from the TCGA-PRAD cohort, differential expression analysis was conducted using the DESeq2 package based on raw count data. DESeq2 internally normalizes count data using size factors and models gene expression using a negative binomial distribution. Genes with $|\log_2 FoldChange|>1$ and adjusted $P<0.05$ were considered significantly differentially expressed. For microarray data from GSE32571 and GSE3325, the limma package (version 3.54.2, https://bioconductor.org/packages/release/bioc/html/limma.html) was used to construct linear models, and differential expression was calculated after empirical Bayes moderation. Finally, lists of upregulated and downregulated DEGs were obtained for each dataset.

GO and KEGG enrichment analyses. After loading DEGs into the R environment, functional annotation analysis was performed using the 'clusterProfiler' package (19). GO functional annotation: Enrichment tests were conducted separately for three dimensions, namely biological process (BP), cellular component (CC) and molecular function (MF). P-values were calculated based on hypergeometric distribution tests, significant terms were screened by combining gene count thresholds, and the FDR was controlled using the Benjamini-Hochberg method. KEGG signaling pathway analysis: The pathway mapping function of clusterProfiler was used to analyze the metabolic and signal transduction networks involved in DEGs. A dual screening criterion of $P<0.05$ and $FDR<0.1$ was set to ensure both biological significance and statistical rigor. Visualization of expression patterns: A two-color gradient heatmap was generated using the 'pheatmap' package (20), with tumor samples and normal tissues compared in separate columns; red modules indicated upregulated gene clusters, and blue modules indicated downregulated gene clusters. Row clustering was performed using the correlation coefficient distance algorithm. The built-in plotting function of 'clusterProfiler' (21) was called, where the bubble area reflected the number of genes covered by each term, and the color gradient depth corresponded to the $-\log_{10}$(P-value) intensity; significantly enriched terms were concentrated in the upper left area of the chart.

Lasso regression analysis. Lasso regression analysis was performed using the 'glmnet' package in R to screen DEGs related to PC prognosis. The parameter α was set to 1 (Lasso mode), and 10-fold cross-validation was used to optimize the regularization strength λ. In the coefficient profile plot, as the λ value increased (x-axis: Log Lambda), the number of genes with non-zero coefficients gradually decreased. Finally, the λ value corresponding to the point with the smallest deviation was selected, and genes with non-zero coefficients were identified as prognosis-related candidate genes.

Univariate and multivariate cox regression analyses. The 20 genes screened by Lasso were included in survival analysis, and the 'survival' package (22) was used to construct a univariate Cox proportional hazards model. With patients' disease-free survival (DFS) as the endpoint event, the risk coefficient (coef) and P-value of each gene were calculated, and genes with P<0.05 were screened as potential prognostic biomarkers. To eliminate the interference of confounding factors, genes that were significant in the univariate analysis and clinicopathological parameters (age, staging) were jointly included in a multivariate Cox model. Stepwise regression was used to identify independent prognostic factors.

Construction of risk model and verification by survival analysis. Based on the expression profiles of the 9 independent prognostic genes, a risk scoring model (Riskscore) was constructed using a linear weighted method. Patients were divided into high/low-risk groups according to the median risk score. The 'survival' package was used to draw Kaplan-Meier curves, and the log-rank test was used to compare survival differences between groups. Model verification: The 'timeROC' package (23) was used to draw 1-year, 3-year, and 5-year time-dependent receiver operating characteristic (ROC) curves, and the area under the curve (AUC) value was calculated to evaluate the prediction accuracy of the model.

Cell culture. Human PC cell lines (DU145, LNCaP and PC-3), murine PC line (RM-1) and a normal prostate epithelial cell line (RWPE-1) were cultured in RPMI-1640 medium (cat. no. 11875093; Thermo Fisher Scientific, Inc.) supplemented with 10% fetal bovine serum (FBS; cat. no. 10099-141C; Gibco; Thermo Fisher Scientific, Inc), under the conditions of 37˚C and 5% CO_2. Cells were digested and passaged with 0.25% trypsin every 2-3 days to maintain a cell density of 70-80% confluence. All cell lines were purchased from the Chinese Academy of Medical Sciences.

Gene intervention. Cell models with transient knockdown or overexpression of SRRT were established in DU145 and PC-3 cell lines, respectively. For knockdown experiments, SRRT-siRNA (si-SRRT) and negative control (si-NC) were transfected using Lipofectamine 3000 reagent. For overexpression experiments, overexpression vector (OE-SRRT) and empty vector (NC) were transfected. The transfection reagent was Lipofectamine 3000 (cat. no 455560) from Invitrogen; Thermo Fisher Scientific, Inc. A total of 24 h before transfection, cells were seeded in 6-well plates at a density of $2x10^5$ cells/well. Tube A (containing 50 μl Opti-MEM and 5 μl Lipofectamine 3000 per well) and Tube B [containing 50 μl Opti-MEM and 2.5 μg small interfering RNA (siRNA) per well] were prepared separately, mixed, and incubated at room temperature for 15 min, then added to the cells. After 6 h, the medium was replaced with complete medium, and cells were collected for RNA or protein extraction 48 h after transfection. The overexpression vector pCDNA3.1-SRRT (OE-SRRT; pcDNA3.1 vector: Invitrogen; Thermo Fisher Scientific, Inc.) and empty vector (NC) were verified by sequencing. For their transfection, the preparation of Tube A (50 μl Opti-MEM + 5 μl Lipofectamine 3000 per well) and Tube B (50 μl Opti-MEM + 2.5 μg plasmid per well) and subsequent steps were the same as those for siRNA transfection. The siRNA sequences are shown as follows: si-SRRT-1 sense, 5'-CAGUUCUAAUGAUGACAAAAC-3' and antisense, 5'-UUUGUCAUCAUUAGAACUGUC-3'; si-SRRT-2 sense, 5'-CGCAAAACCCGAUCUUGAAGA-3' and antisense, 5'-UUCAAGAUCGGGUUUUGCGAG-3'; and si-NC sense, 5'-UUCUCCGAACGUGUCACGU-3' and antisense, 5'-ACGUGACACGUUCGGAGAA-3'.

Western blotting. Total protein was extracted using RIPA lysis buffer (Beyotime Institute of Biotechnology) supplemented with protease inhibitor cocktail (Roche Diagnostics) and phosphatase inhibitors, according to the manufacturer's instructions. Total protein was quantified using the BCA method. Equal amounts of protein (20-30 μg per lane) were loaded onto 10% SDS-PAGE gels, separated by electrophoresis, and then transferred to a PVDF membrane, which was then blocked with 5% bovine serum albumin (Beyotime Institute of Biotechnology) for 1 h at room temperature. Primary antibodies against SRRT (1:1,000; cat. no. 20353-1-AP), STAT3 (1:1,500; cat. no. 10253-2-AP), phosphorylated (p-) STAT3 (1:1,000; cat. no. 28945-1-AP) and GAPDH (1:3,000; cat. no. 10494-1-AP; all from Proteintech Group, Inc.) were used for incubation at 4˚C overnight, followed by incubation with HRP-conjugated secondary antibody (1:5,000; cat. no. 31460; Thermo Fisher Scientific, Inc.) at room temperature for 1 h the next day. Enhanced chemiluminescence (cat. no. P0018M; Beyotime Institute of Biotechnology) development was performed, and the gray value was quantified using ImageJ software (version: 1.42q; National Institutes of Health). GAPDH was used as the internal reference to calculate the relative expression level. All Western blot experiments were performed with at least three independent biological replicates (n=3).

Immunohistochemistry (IHC). Adjacent benign and PC tissue specimens from 70 patients with PC (all male, median age 71 years, range 51-84 years) were collected and processed according to established histopathological protocols (24). Briefly, tissues were fixed in 10% neutral-buffered formalin at room temperature for 24 h, embedded in paraffin, and sectioned at a thickness of 4 μm. IHC was performed as previously described (25,26) to evaluate SRRT expression. After deparaffinization and rehydration, antigen retrieval was carried out in citrate buffer (pH 6.0) using microwave heating. Endogenous peroxidase activity was quenched with 3% hydrogen peroxide, followed by blocking with normal serum for 30 min at room temperature. The sections were then incubated overnight at 4˚C with primary antibody against SRRT (1:1500; cat. no. 20353-1-AP; Proteintech Group, Inc). The present study was approved (approval no. KY-H-2023-039-01) by the Ethics Committee of Soochow University (Suzhou, China) and followed the principles outlined in the Declaration of Helsinki. Written informed consent was obtained from all patients.

Subsequently, the slides were processed using the streptavidin-biotin-peroxidase method, with diaminobenzidine (DAB) as the chromogen, and counterstained with hematoxylin. Negative controls were included in each run by omitting

the primary antibody or substituting it with isotype-matched irrelevant antibodies to confirm staining specificity.

IHC staining was independently evaluated by two observers, including an experienced pathologist, who were blinded to the clinical data. Discrepancies were resolved by joint review to reach a consensus. SRRT expression levels were semi-quantitatively scored based on both staining intensity (0=none, 1=weak, 2=moderate, 3=strong) and the percentage of positive tumor cells (0=0%, 1=1-25%, 2=26-50%, 3=>50%). The final immunoreactivity score was calculated by summing these two parameters and classified as negative (0), weak (1-2), moderate (3-4), or strong (5-6) (27).

CCK-8 assay. Cells were seeded in 96-well plates at a density of 3,000 cells/well, and after 24 h of culture, the medium was replaced with medium containing different treatment factors. A total of 10 microliters of CCK-8 reagent (cat. no. C0037; Beyotime Institute of Biotechnology) was added to each well, followed by incubation at 37˚C for 2 h. The absorbance (OD value) at 450 nm was measured using a microplate reader. Wells without cells were used for zero adjustment, and cell viability was calculated according to the formula: (OD of treatment group/OD of control group x100%). Each experimental condition was performed in triplicate wells and independently repeated at least three times (n=3).

Transwell assay. For the migration assay, Transwell inserts with an 8-μm pore size were used. 200 μl of serum-free medium containing $5x10^4$ cells was added to the upper chamber of the Transwell, and 600 μl of medium containing 20% FBS was added to the lower chamber. After 24 h of culture at 37˚C, non-migratory cells in the upper chamber were wiped off with a cotton swab. Cells in the lower chamber were fixed with 4% paraformaldehyde for 15 min at room temperature, stained with 0.1% crystal violet for 15 min at room temperature, and images were captured using a light microscope (x100), and the number of migratory cells in 5 random fields was counted. Each experiment was independently repeated at least three times (n=3).

Scratch assay. Cells were seeded in 6-well plates until reaching 90% confluence, then scratched vertically with a 200-μl pipette tip. Cells were washed 3 times with PBS to remove floating cells, and the medium was replaced with serum-free medium for further culture. Images were captured under a light microscope (x40) at 0 and 48 h, respectively. The scratch healing area was measured using ImageJ software, and the healing rate was calculated according to the formula: [(Initial area-Remaining area)/Initial area x100%]. All experiments were conducted in triplicate and repeated independently at least three times (n=3).

In vivo tumor growth assay. A total of 16 male BALB/c athymic nude mice (6 weeks old′ weighing 20-22 g at the start of the experiment) were subcutaneously injected with either control or SRRT-overexpressing PC cells. Mice were randomly divided into two groups (n=8 per group). For the tumor growth assay, $1x10^6$ cells suspended in 100 μl PBS were inoculated subcutaneously into six-week-old mice. All mice were maintained under specific pathogen-free conditions at a constant temperature of 25˚C, relative humidity of 40-70%, with a 12/12-h light/dark cycle and free access to food and water. Tumor dimensions were measured every 3 days before tumor formation became evident, and once tumors were detectable, measurements were performed daily. Tumor volumes were calculated using the formula: Length x width^2 x 0.5 (mm^3). Humane endpoints were predefined: animals were euthanized if tumor size exceeded 15 mm in any dimension or if tumor weight reached 10% of the body weight. If these criteria were not met, all mice were sacrificed at 54 days post-injection. Mice were euthanized by CO_2 asphyxiation at a flow rate of 35% chamber volume per minute and were exposed to CO_2 for at least 1 additional min after cessation of breathing. Death was confirmed by cessation of heartbeat and respiration, as well as physical signs including body stiffness and dilated pupils. No animals were excluded from the analysis. All animal experiments were approved by the Ethics Committee of Suzhou Ninth People's Hospital (approval no. KY2023-039-01; Suzhou, China) and were conducted in accordance with relevant institutional and national guidelines. Our study was reported as described by the ARRIVE guidelines.

Statistical analysis. Statistical analyses were performed using R (version 4.1.0; R Foundation for Statistical Computing; https://www.r-project.org/) and GraphPad Prism (v9.0.0; Dotmatics). For TCGA-PRAD data, specific software packages and statistical methods were applied for screening DEGs, conducting enrichment analyses, and identifying prognostic genes. Experimental data were presented as the mean ± standard deviation. Comparisons between two groups were analyzed using an unpaired Student's t-test, while comparisons among multiple groups were performed using one-way analysis of variance (ANOVA) followed by Tukey's post hoc test. $P<0.05$ was considered to indicate a statistically significant difference.

Results

Exploration of DEGs in PC based on multiple datasets. To identify DEGs associated with PC, differential expression analyses were performed across multiple datasets. In the TCGA-PRAD dataset, volcano plots and heatmaps revealed distinct expression patterns between tumor and adjacent normal tissues (Fig. 1A and B). Similar differential expression patterns were observed in the GSE32571 dataset (Fig. 1C and D) and the GSE3325 dataset (Fig. 1E and F). By integrating the results from TCGA-PRAD, GSE32571 and GSE3325, a total of 85 commonly upregulated and 10 commonly downregulated DEGs were identified through overlap analysis (Fig. 1G and H), providing a reliable basis for subsequent analyses.

GO and KEGG enrichment analyses. To investigate the molecular functional characteristics of DEGs and the key biological processes they participate in, GO biological process enrichment analysis and KEGG pathway enrichment analysis were performed on the commonly upregulated DEGs from the three datasets. The results of GO biological process enrichment showed significantly enriched biological processes, such

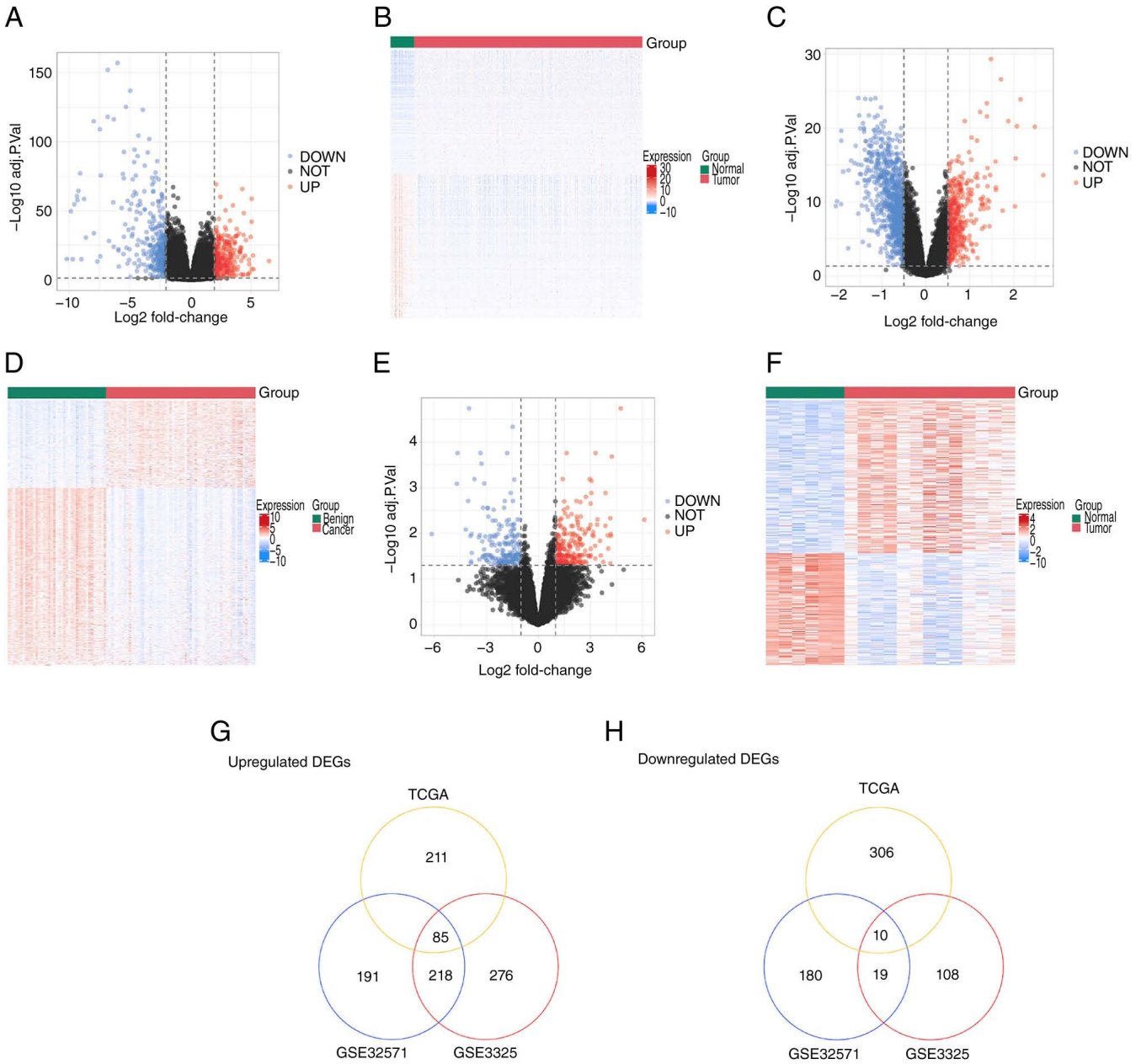

Figure 1. Comprehensive analysis of DEGs in PC. (A) Volcano plot of DEGs between PC and adjacent normal tissues in the TCGA-PRAD dataset; the x-axis represents the fold change in gene expression, the y-axis represents statistical significance, and red dots indicate genes with significant differences. (B) Heatmap of DEGs between PC and adjacent normal tissues in the TCGA-PRAD dataset; red indicates high expression, and blue indicates low expression. (C) Volcano plot of DEGs between PC and adjacent normal tissues in the GSE32571 dataset. (D) Heatmap of DEGs between PC and adjacent normal tissues in the GSE32571 dataset. (E) Volcano plot of DEGs between PC and adjacent normal tissues in the GSE3325 dataset. (F) Heatmap of DEGs between PC and adjacent normal tissues in the GSE3325 dataset. (G) Commonly upregulated DEGs across the three datasets (TCGA-PRAD, GSE32571 and GSE3325). (H) Commonly downregulated DEGs across the three datasets (TCGA-PRAD, GSE32571 and GSE3325). DEGs, differentially expressed genes; PC, prostate cancer; TCGA, The Cancer Genome Atlas;

as carboxylic acid biosynthesis and organic acid metabolism (Fig. 2A). The results of KEGG signaling pathway enrichment highlighted key pathways, including the STAT3 signaling pathway and drug metabolism (Fig. 2B). This analysis provides directions for subsequent mechanistic studies.

Screening of independent prognostic genes for PC. To construct a robust prognostic signature, LASSO regression was first applied to the 85 upregulated DEGs, yielding 20 candidate genes with potential prognostic relevance. These candidates were subsequently subjected to univariate and multivariate Cox regression analyses, resulting in the identification of nine independent prognostic genes. The LASSO model demonstrated effective coefficient shrinkage with increasing penalty parameter (λ), and cross-validation analysis was used to determine the optimal model complexity (Fig. 3A and B). The final prognostic model incorporated nine genes, each of which assigned a corresponding regression coefficient (Fig. 3C). Among them, SRRT exhibited the largest coefficient, indicating its prominent contribution to the risk score and a stronger association with unfavorable clinical outcomes in PC.

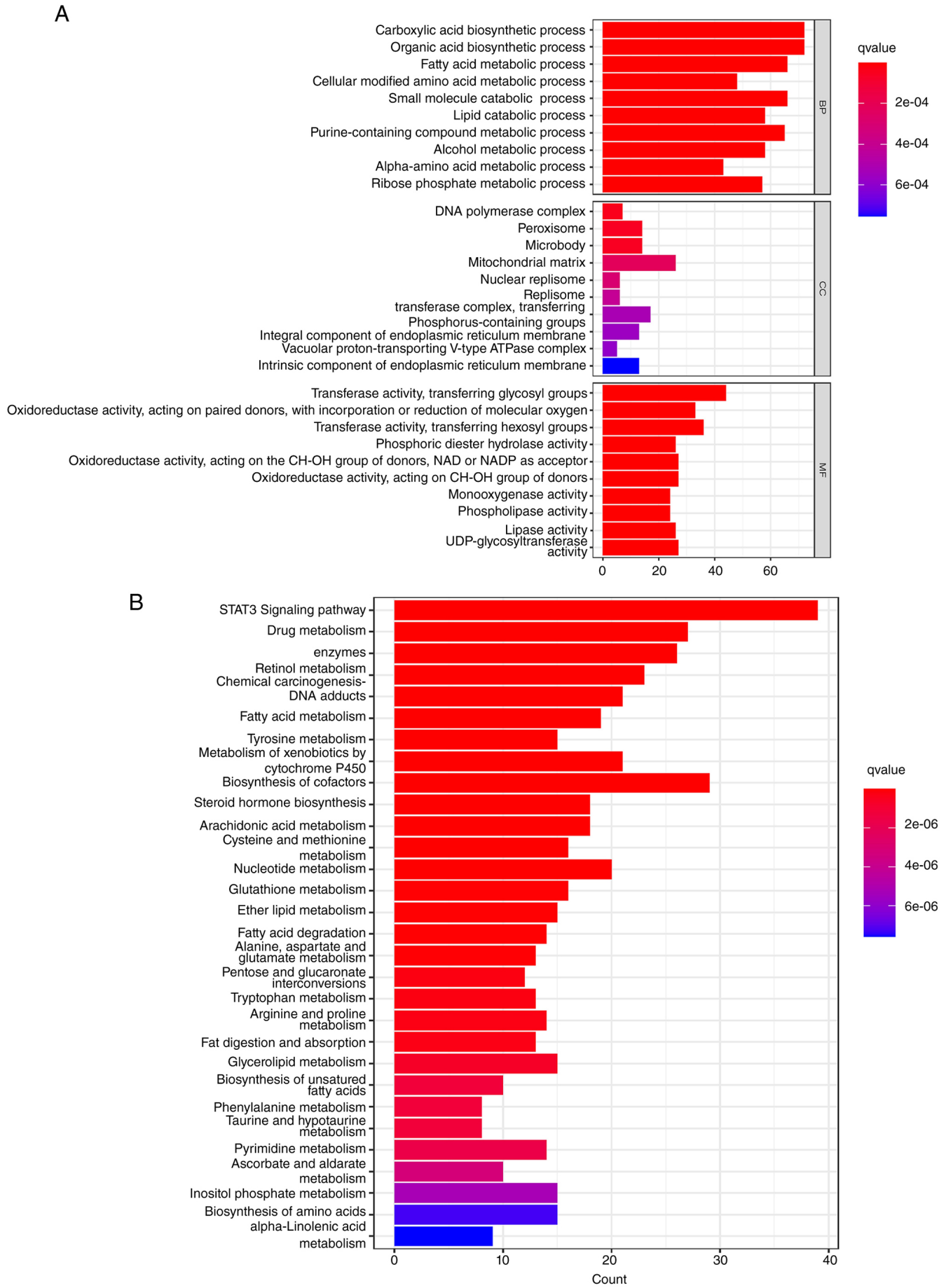

Figure 2. Functional enrichment analysis of common differentially expressed genes. (A) Bar plot of Gene Ontology biological process enrichment. (B) Bar plot of Kyoto Encyclopedia of Genes and Genomes pathway enrichment.

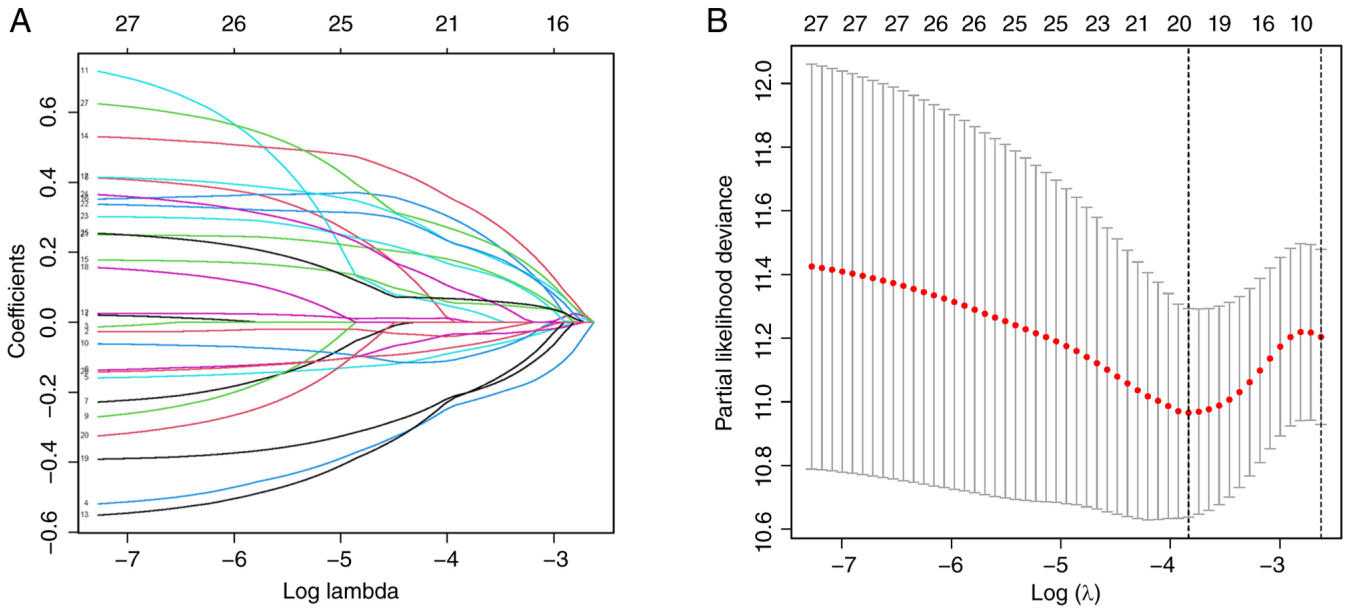

C

Gene	Coefficient (coef)	Hazard ratio (HR)
SLC4A4	−0.545	0.58
PPARGC1A	−0.547	0.579
SRRT	0.618	1.856
TIGD1	0.496	1.643
FOXD1	0.388	1.474
TRIP6	0.268	1.308
OSBPL3	0.472	1.603
PCDHB14	0.368	1.445
TIMP1	0.458	1.581

Figure 3. Screening of independent prognostic genes for PC. (A) Coefficient profile plot of Lasso regression, showing the trend of gene coefficient changes with Log Lambda; different colored curves represent the coefficient change trends of different genes, reflecting the effect of the penalty parameter on gene coefficients. (B) Cross-validation plot of Lasso regression; the y-axis represents the deviation, the x-axis represents Log (λ), and the dashed lines indicate the λ value corresponding to the minimum deviation and the λ value under the 1-SE criterion, respectively, which are used to select the optimal penalty parameter. (C) Table of coefficients of the nine prognostic genes included in the risk model. SRRT had the highest coefficient, suggesting its potential key role in PC prognosis. PRAD, prostate cancer.

Efficacy verification of the constructed risk model. Kaplan-Meier survival analysis and time-dependent ROC curve analysis were performed to evaluate the prognostic performance of the risk model. The results showed that patients in the high-risk group had significantly poorer DFS compared with those in the low-risk group in both the TCGA cohort and the GSE3325 validation dataset (Fig. 4A and B; P<0.001). Consistently, risk distribution analysis indicated that events occurred earlier and more frequently in the high-risk group.

Time-dependent ROC analysis demonstrated that the model achieved AUC values of 0.78, 0.82 and 0.85 at 1, 3 and 5 years, respectively (Fig. 4C and D), indicating favorable predictive performance over time. These findings suggest that the risk score may serve as a useful indicator for prognostic stratification in PC.

Construction and evaluation of a nomogram for individualized prognostic prediction. To further assess the clinical applicability of the model, a nomogram integrating SRRT-based risk score with clinicopathological variables (race, stage, T stage, N stage, grade and age) was constructed to predict 1-, 3- and 5-year DFS probabilities. Calibration curves demonstrated favorable agreement between predicted and observed outcomes across all time points (Fig. 4E), indicating acceptable predictive accuracy.

The nomogram (Fig. 4F) enabled estimation of individual patient risk by assigning weighted scores to each variable and calculating total points, which were subsequently translated into corresponding DFS probabilities. Overall, these results suggest that the integrated model may provide a quantitative approach for individualized prognostic assessment, although its clinical utility requires further validation.

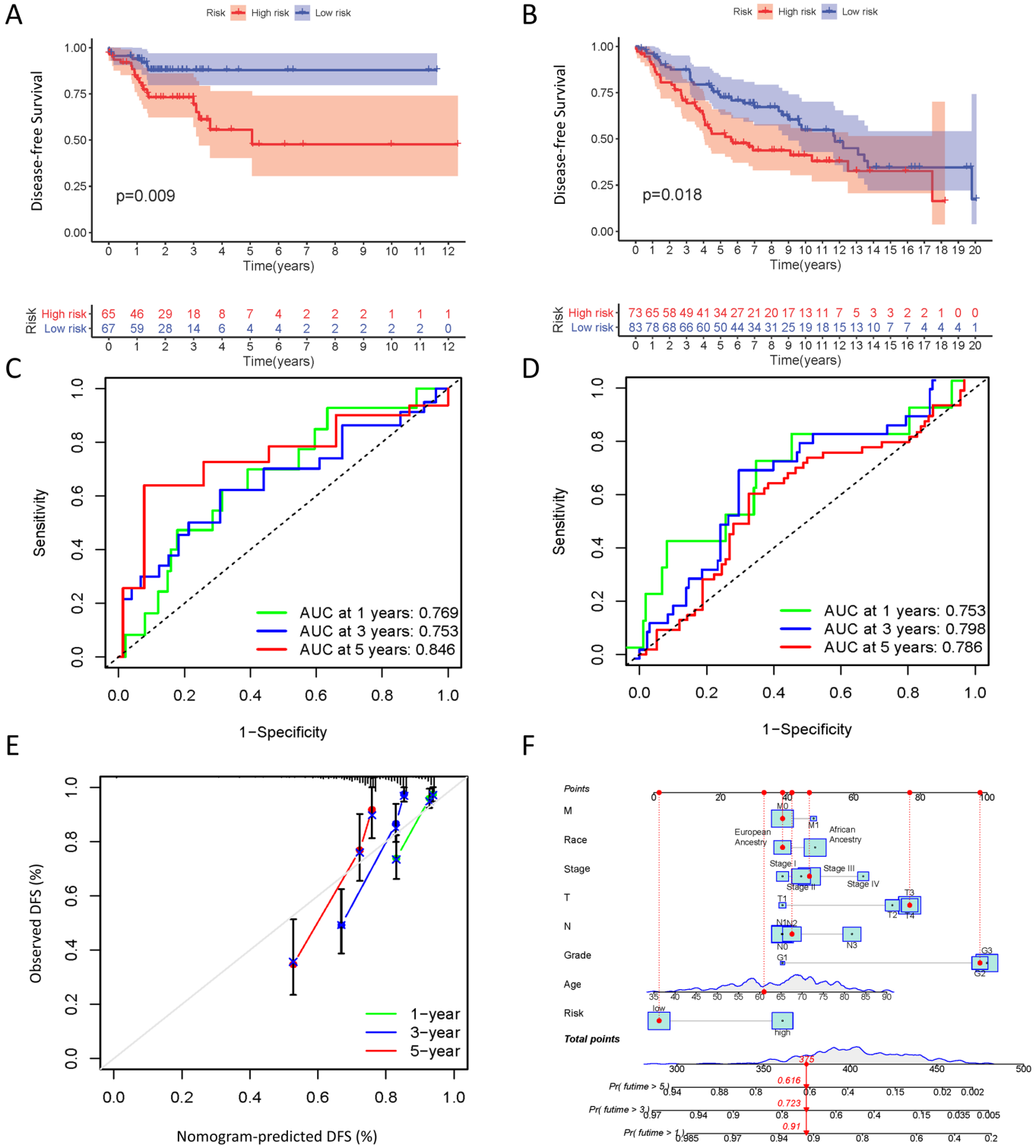

Figure 4. Verification analysis, calibration and visualization of the prognostic model. (A and B) Kaplan-Meier curves of DFS for high- and low-risk groups. Red represents the high-risk group, and blue represents the low-risk group. P<0.05 indicates a statistically significant difference in survival between the groups. The risk table below shows the number of surviving patients at each time point. (C and D) Time-dependent Receiver Operating Characteristic curves showing the predictive performance of the model at 1, 3 and 5 years. (E) Calibration plots for 1-, 3- and 5-year DFS, comparing predicted and observed outcomes. (F) Nomogram for predicting 1-, 3- and 5-year DFS based on the risk score and clinicopathological variables. DFS, disease-free survival; AUC, area under the curve.

Functional verification of SRRT in PC. To explore the biological role of SRRT in PC, *in vitro* functional verification experiments were performed. Western blot results showed that compared with the normal cell line RWPE-1, SRRT was highly expressed in the PC cell lines DU145 and PC-3 (Fig. 5A). IHC staining of PC samples further validated these findings, identifying significantly elevated SRRT protein levels in tumor tissues relative to benign controls (Fig. 5B). Further siRNA knockdown experiments revealed that the protein levels of SRRT in DU145 and PC3 cells were significantly reduced,

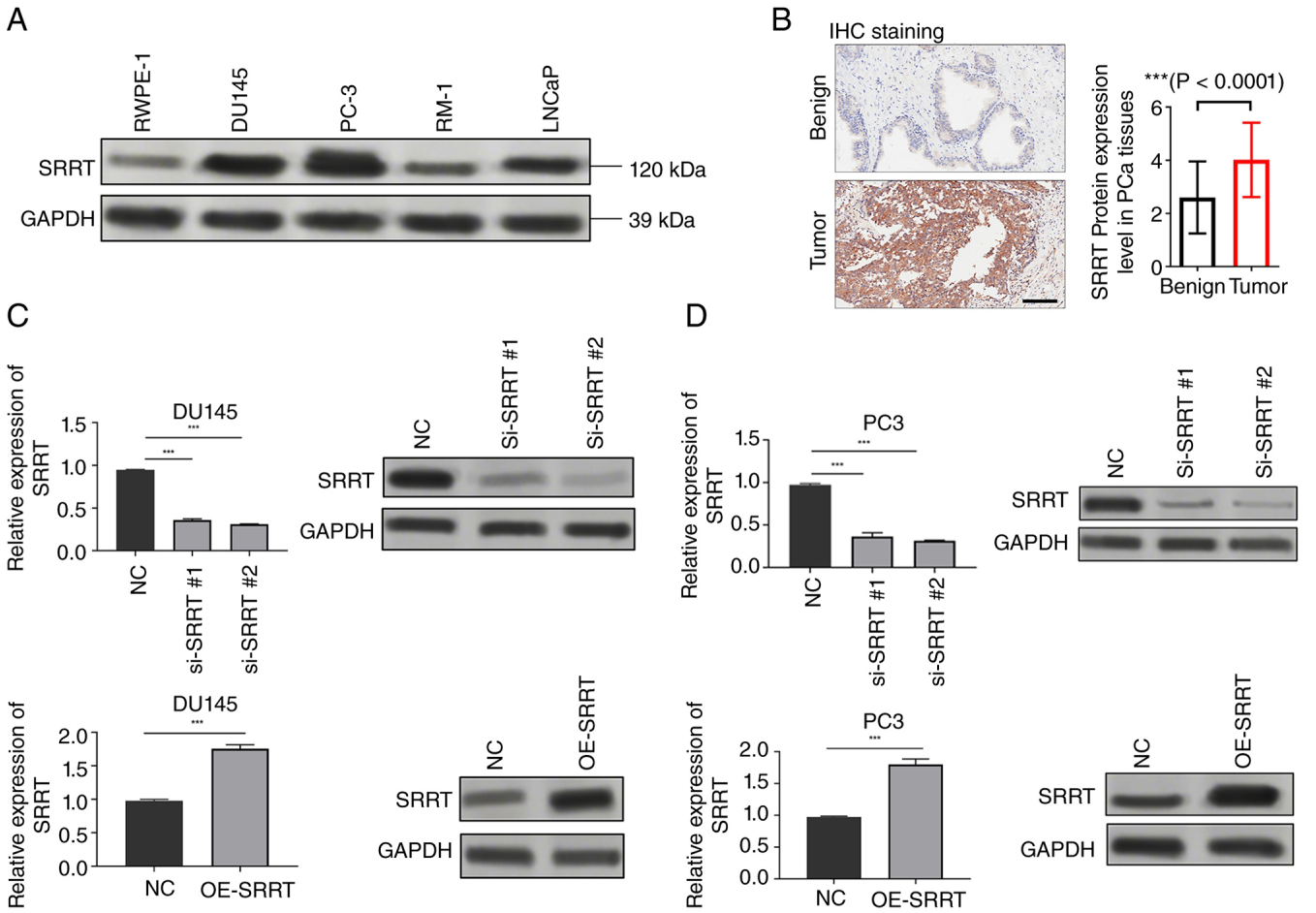

Figure 5. Verification of SRRT expression and regulation in PC. (A) Western blot analysis of SRRT expression differences between PC cell lines and the normal prostate epithelial cell line (RWPE-1). GAPDH was used as the internal reference for normalization. (B) Representative IHC staining of SRRT in benign and prostate cancer tissues, with quantitative scoring confirming higher SRRT protein expression in tumors (Scale bars, 100 μm). (C and D) Western blot was used to verify the knockdown or overexpression efficiency in (C) DU145 and (D) PC3 cells. Changes in protein expression were detected. Specific siRNAs (Si-SRRT#1 and #2) were designed and transfected into cells, with a non-targeting siRNA (Si-NC) as the control. SRRT OE vectors (OE-SRRT) were constructed and transfected into cells, with an empty vector (NC) as the control. ***P<0.0001. PC, prostate cancer; IHC, immunohistochemistry; siRNA, small interfering RNA; NC, negative control; OE, overexpression.

while overexpression experiments increased the expression of SRRT in both cell lines (Fig. 5C and D). These results confirm that SRRT can be effectively regulated in PC cells, providing an experimental basis for subsequent functional and mechanistic studies.

Regulatory role of SRRT in the proliferation of PC cells. To verify the effect of SRRT on the proliferation of PC cells, CCK-8 proliferation curves showed that after SRRT knockdown or overexpression in DU145 cells, the cell proliferation ability was significantly decreased or increased, respectively (Fig. 6A and B). This finding was further confirmed in the PC-3 cell line and the same results were obtained after SRRT knockdown or overexpression (Fig. 6C and D). To assess the effects *in vivo*, a xenograft tumor model was generated using DU145 cells in male BALB/c athymic nude mice (n=16). Subcutaneous xenograft assay confirmed that SRRT-OE led to significantly increased tumor volume over time and greater final tumor weight compared with controls (Fig. 6E). The maximum tumor volume observed in the present study was 1,485.3 mm^3, with a corresponding maximum tumor diameter of 14.4 mm, both of which were within the predefined humane endpoint criteria. These results suggest that SRRT may participate in the progression of PC by promoting cell proliferation in androgen-independent PC models.

SRRT could promote the migration ability of PC cells. To further investigate the role of SRRT in regulating the migratory capacity of PC cells, Transwell and wound healing assays were performed. SRRT knockdown significantly reduced the migration of DU145 and PC-3 cells, as demonstrated by the Transwell assay (Fig. 7A), which was further confirmed by wound healing analysis (Fig. 7B). By contrast, SRRT overexpression significantly enhanced the migratory ability of both cell lines (Fig. 7C) and accelerated scratch closure at 48 h, indicating increased cell motility (Fig. 7D). Collectively, these results suggest that SRRT may enhance the migratory ability of PC cells.

SRRT promotes PC progression via the STAT3 pathway. Finally, the potential mechanism by which SRRT promotes the progression of PC was further explored. KEGG pathway analysis revealed that the STAT3 signaling pathway was the most significantly enriched, prompting us to investigate its

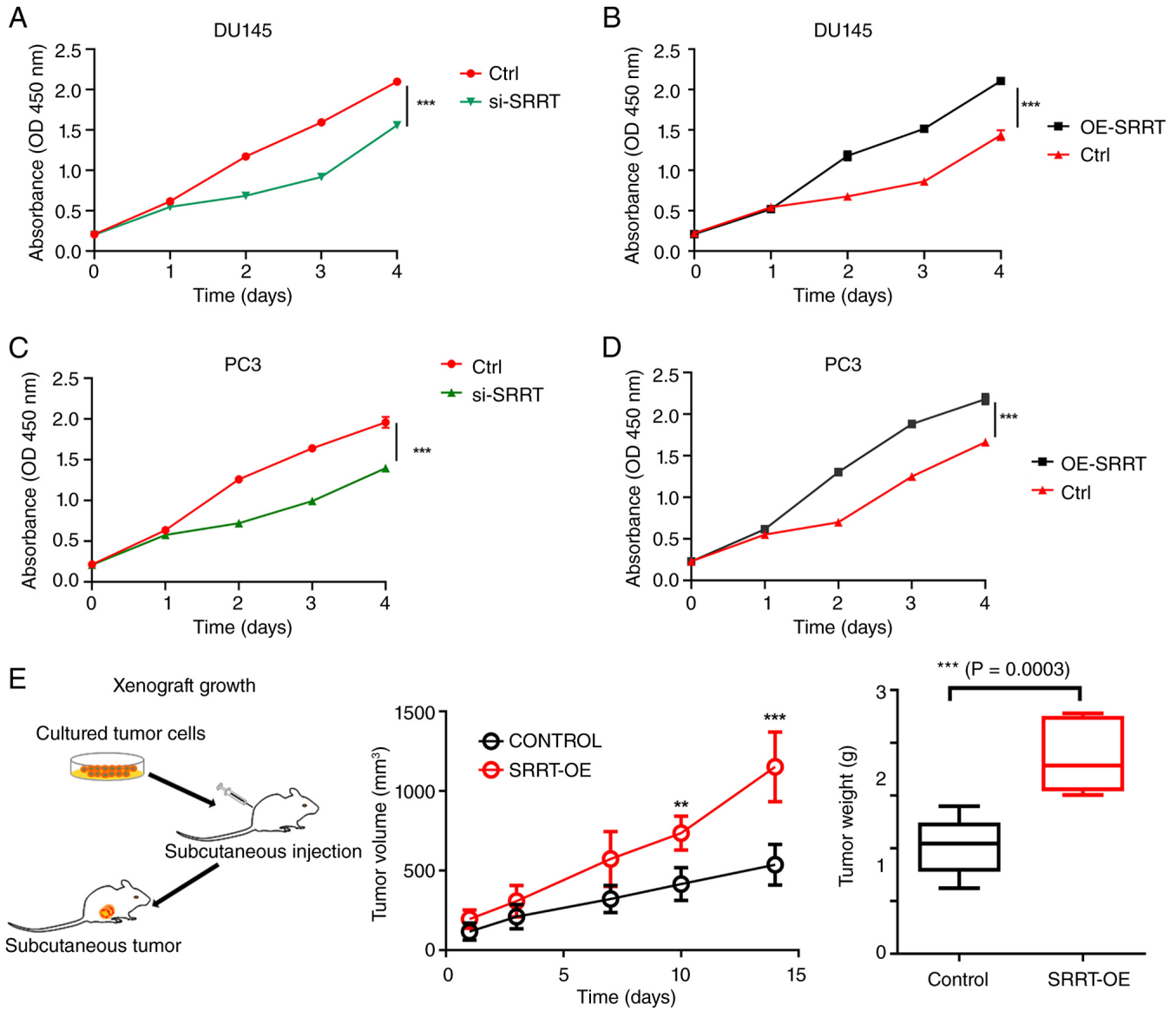

Figure 6. Regulatory role of SRRT in the proliferation of prostate adenocarcinoma cells. (A-D) Trends of OD450 values over time in (A and B) DU145 and (C and D) PC3 cells after SRRT knockdown (si-SRRT) or OE (OE-SRRT). (E) Xenograft analyses of DU145-derived tumors with control vector or SRRT OE. **P<0.01 and ***P<0.001. si-, small interfering; OE, overexpression.

involvement. Western blot analysis demonstrated that SRRT expression markedly affected the phosphorylation status of key proteins in the STAT3 pathway. In DU145 cells (Fig. 8A), SRRT knockdown significantly reduced the p-STAT3/STAT3 ratio, whereas SRRT overexpression increased this ratio in both cell lines. To further validate the mediating role of STAT3 signaling in SRRT-induced tumor promotion, SRRT-silenced DU145 cells were treated with the STAT3 activator colivelin (0.5 μM) and it was found that colivelin partially restored the reduced p-STAT3/STAT3 ratio caused by SRRT knockdown (Fig. 8B). Moreover, cell proliferation and migration assays revealed that colivelin treatment rescued the inhibitory effects of SRRT silencing on these cellular behaviors (Fig. 8C and D). These findings suggest that SRRT promotes PC progression by activating the STAT3 signaling pathway, particularly in androgen-independent cellular models, further confirming that SRRT serves as an important upstream regulator of STAT3 signaling.

Discussion

The malignant progression and prognostic heterogeneity of PC are orchestrated by multiple genes and signaling pathways. Identifying molecular determinants with prognostic relevance and potential biological significance remains a central challenge in PC research (28,29). Through integrated bioinformatics analysis and *in vitro* validation, the present study systematically characterized the expression pattern, prognostic significance and regulatory mechanism of SRRT in PC, providing new insights for precise diagnosis and molecular stratification of patients.

At the bioinformatics level, data from the TCGA-PRAD and GEO (GSE32571 and GSE3325) datasets were combined, identifying 85 commonly upregulated and 10 commonly downregulated DEGs (30). Cross-validation across datasets minimized potential bias and technical variability, thereby enhancing the robustness of th present findings. GO

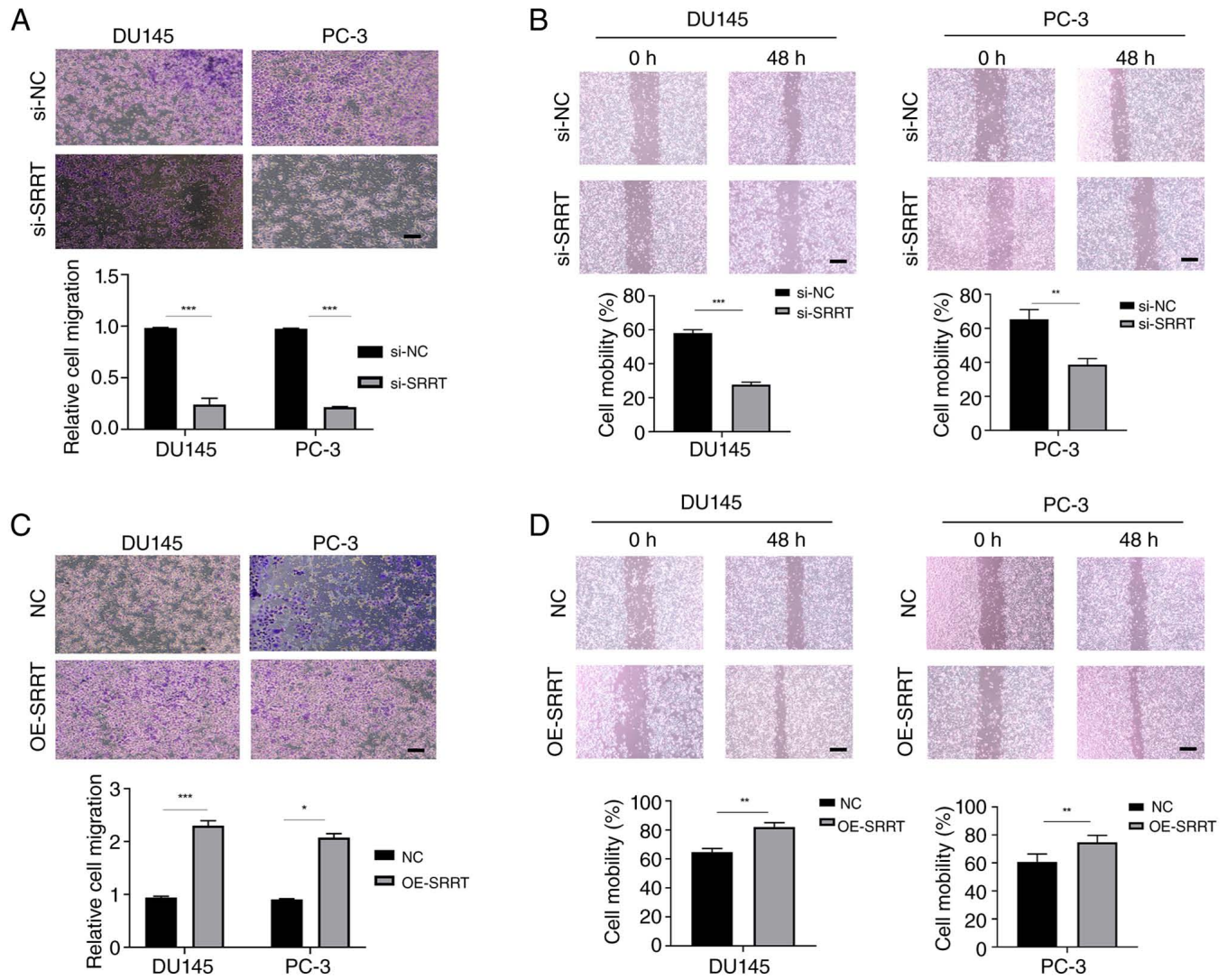

Figure 7. *In vitro* verification of SRRT regulating the migration of prostate adenocarcinoma cells. (A) Migration of DU145 and PC3 cells after treatment with si-NC or si-SRRT (scale bars, 50 μm). (B) Scratch healing of DU145 and PC3 cells after treatment with si-NC or si-SRRT at 0 and 48 h under a microscope (Scale bars, 100 μm). (C) Observations of cell migration abilities after SRRT overexpression in DU145 and PC3 cell lines, respectively (Scale bars, 50 μm). (D) Scratch healing of DU145 and PC3 cells after treatment with NC or OE-SRRT at 0 and 48 h under a microscope (Scale bars, 100 μm). *P<0.05, **P<0.01 and ***P<0.001. si-, small interfering; OE, overexpression; NC, negative control.

enrichment analysis showed that the upregulated DEGs were mainly involved in carboxylic acid biosynthesis and organic acid metabolism-biological processes closely related to tumor metabolic reprogramming, a well-recognized hallmark of malignancy (31,32). Furthermore, KEGG pathway analysis highlighted significant enrichment of the STAT3 signaling pathway. Persistent activation of STAT3 has been shown to promote PC proliferation and migration by regulating downstream targets such as Cyclin D1 and MMP-9 (33,34), supporting our focus on STAT3 in subsequent mechanistic studies.

To identify prognosis-related DEGs, Lasso regression analysis was performed, followed by univariate and multivariate Cox analyses, which identified nine independent prognostic genes. Among these, SRRT exhibited the highest risk coefficient, indicating a strong association with unfavorable survival outcomes. The prognostic model constructed from these genes demonstrated high predictive accuracy in both TCGA and GEO cohorts, with a 5-year AUC of 0.85 (35,36). Moreover, the nomogram integrating SRRT expression with clinicopathological parameters (for example, age, TNM stage) achieved excellent calibration, providing a potentially useful tool for risk stratification, although its added value beyond standard clinicopathological models requires further validation (37). In this context, SRRT may help identify patients with biologically aggressive disease, particularly in the context of androgen-independent PC, who are at higher risk of progression and may benefit from closer surveillance or more intensive management strategies. From a clinical perspective, such molecular stratification could complement existing clinicopathological factors (for example, stage and grade) and improve risk classification, particularly in patients with heterogeneous disease courses. This may be especially relevant for distinguishing patients who are less suitable for active surveillance or those who require closer follow-up after definitive treatment. However, these potential applications remain speculative and require validation in well-defined clinical cohorts. Future studies

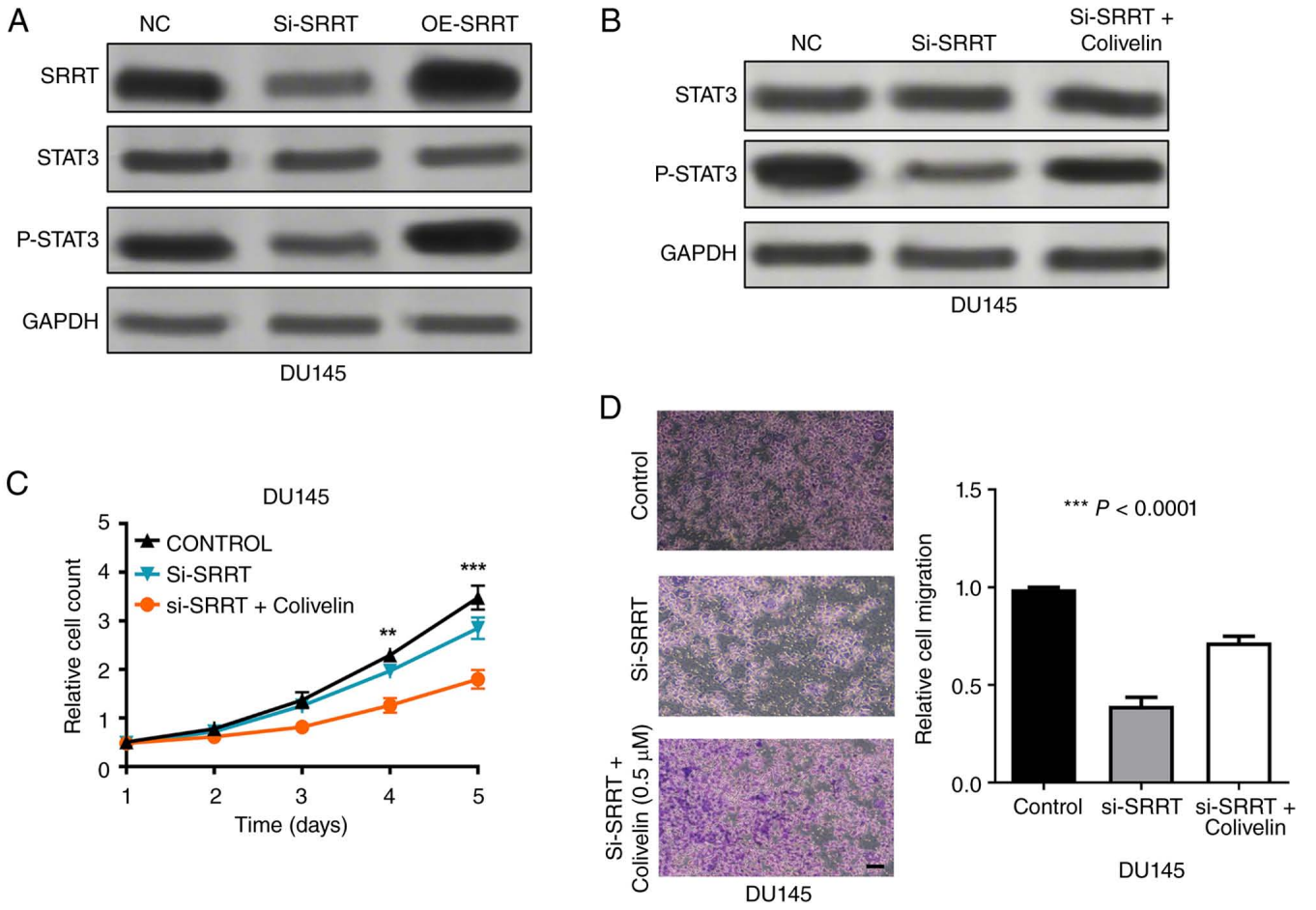

Figure 8. Regulation of key protein expression in the STAT3 pathway by SRRT. (A) Western blot analysis of the expression of SRRT, p-STAT3, STAT3 and the internal reference protein GAPDH in different treatment groups of the DU145 cell line. (B) Protein expression of SRRT, p-STAT3 and STAT3 in control and SRRT-knockdown DU145 cells treated with colivelin. (C) Cell Counting Kit-8 assay evaluating the proliferative capacity of control and SRRT-knockdown DU145 cells treated with colivelin. (D) Transwell migration assay assessing the migratory ability of control and SRRT-knockdown DU145 cells following colivelin treatment (Scale bars, 50 μm). **P<0.01 and ***P<0.001. p-, phosphorylated; si-, small interfering; NC, negative control.

should compare models with and without SRRT to determine whether it provides meaningful improvement in predictive performance and clinical utility.

Functional experiments further confirmed the oncogenic role of SRRT. Western blotting showed that SRRT was markedly overexpressed in PC cell lines (DU145 and PC-3) compared with normal prostate epithelial cells (RWPE-1). Silencing SRRT significantly inhibited cell proliferation and migration, whereas SRRT overexpression enhanced these malignant behaviors. Mechanistically, SRRT knockdown reduced, while overexpression increased, the p-STAT3/STAT3 ratio, indicating that SRRT activates STAT3 signaling through enhanced STAT3 phosphorylation. This mechanism aligns with previous findings showing SRRT's involvement in tumor progression via modulation of signaling pathways. For instance, SRRT promotes hepatocellular carcinoma growth through PI3K-AKT pathway activation (16,38). The present study extends current knowledge by linking SRRT to STAT3 pathway activation in PC, providing additional mechanistic insight into its role in cancer progression. Moreover, the data of the present study demonstrate that SRRT promotes cell migration, suggesting a potential role in metastatic progression. Given that the functional experiments were performed in androgen-independent PC cell lines (DU145 and PC-3), which are widely used models of aggressive disease, SRRT may also be relevant to castration-resistant PC. However, the role of SRRT in the development of castration resistance was not directly investigated in the present study and requires further validation in clinically defined cohorts.

Nevertheless, several aspects warrant further investigation. Traditionally, SRRT has been characterized as a serine/arginine-rich splicing factor involved in RNA processing (13,39). However, the current results indicate its involvement in STAT3 activation. Future studies should determine whether SRRT modulates STAT3 phosphorylation indirectly through RNA splicing of the STAT3 transcript or via direct protein-protein interaction. Additionally, the current experiments were conducted in androgen-independent PC cell lines, whereas PC also includes androgen-dependent subtypes. Therefore, the present findings may be more applicable to aggressive or androgen-independent disease contexts rather than the full spectrum of PC. Future studies using androgen-dependent models and *in vivo* systems will be essential to assess the universality of SRRT's oncogenic role across different PC subtypes. Moreover, prospective clinical validation and evaluation in

well-defined patient cohorts will be required to determine the practical utility of SRRT in clinical decision-making. In addition, whether SRRT represents a druggable target or can predict response to STAT3-directed therapies remains to be determined.

The present study also has limitations. First, the bioinformatics analyses were based on retrospective public datasets, which may introduce sample selection bias, and prospective validation in independent clinical cohorts is still lacking. Second, while it was demonstrated that SRRT regulates STAT3 phosphorylation, the precise molecular mechanism underlying their interaction remains to be elucidated. Third, the functional experiments were primarily conducted in androgen-independent PC cell lines, which may limit the generalizability of the present findings across different disease states. Fourth, although DFS was used as a more clinically relevant endpoint, it may still not fully capture key PC-specific outcomes, such as metastasis-free survival or progression to castration-resistant disease. Finally, the current study does not provide direct evidence that SRRT expression can inform clinical decision-making or guide treatment selection, and its clinical utility requires further investigation. In addition, the *in vivo* validation was limited to a single subcutaneous xenograft model based on SRRT overexpression in DU145 cells, which may not fully recapitulate the complexity of PC progression *in vivo*.

In summary, integrated bioinformatics and experimental analyses identified SRRT as a key oncogenic factor in PC. SRRT serves as an independent poor prognostic biomarker and promotes PC cell proliferation and migration by activating the STAT3 signaling pathway. The SRRT-based risk model accurately predicts patient outcomes, and the nomogram integrating SRRT with clinicopathological parameters enables individualized prognostic assessment. Compared with previous studies, the present study provides integrated multi-cohort bioinformatics evidence supporting the prognostic value of SRRT, establishes a risk model incorporating SRRT for patient stratification, and demonstrates its functional role in promoting PC progression through STAT3 pathway activation. Collectively, SRRT represents a biomarker associated with PC progression and may have potential value for risk stratification and clinical decision-making pending further validation. These findings may be particularly relevant to aggressive or androgen-independent PC, although further validation across diverse disease states is required. However, its role as a therapeutic target remains to be established, and further studies are needed to determine whether SRRT provides incremental prognostic value beyond established clinical factors.

Acknowledgements

Not applicable.

Funding

The present study was supported by the Excellent Talent Project of Xuzhou Medical University (grant no. XYFY202422) and the project of promoting health through science and education (grant no. WWK202308).

Availability of data and materials

The data generated in the present study may be found in the Gene Expression Omnibus under accession numbers GSE32571 and GSE3325 or at the following URL: https://www.ncbi.nlm.nih.gov/geo/query/acc.cgi?acc=GSE32571; https://www.ncbi.nlm.nih.gov/geo/query/acc.cgi?acc=GSE3325. The data generated in the present study may be found in The Cancer Genome Atlas under accession number phs000178 or at the following URL: https://portal.gdc.cancer.gov/projects/TCGA-PRAD.

Authors' contributions

LL, ZM and KW conceptualized and designed the study, and drafted the manuscript. ZM and LL acquired funding. ZW, RY and KL acquired data and drafted the manuscript. LL and SG conducted *in vitro* and *in vivo* assays. ZW, RY and FW critically revised the manuscript. KW, ZM and FW conducted statistical analysis and technical support. All authors read and approved the final version of the manuscript. ZM and LL confirm the authenticity of all the raw data.

Ethics approval and consent to participate

The present study was approved by the Ethics Committee of Soochow University (Suzhou, China) and followed the principles outlined in the Declaration of Helsinki for all human (approval no. KY-H-2023-039-01) or animal experimental (approval no. KY2023-039-01) investigations. Written informed consent was obtained from all patients. The present study was reported as described by the ARRIVE guidelines.

Patient consent for publication

Not applicable.

Competing interests

The authors declare that they have no competing interests.

References

1. Lu B, Liu Y, Ji G, Yao Y, Yang Z, Zhu B, Wang L, Dong K, Li Y, Shi J, *et al*: Construction of a prostate adenocarcinoma molecular classification: Integrating spatial transcriptomics with retrospective cohort validation. J Transl Med 23: 717, 2025.
2. Raychaudhuri R, Lin DW and Montgomery RB: Prostate cancer: A review. JAMA 333: 1433-1446, 2025.
3. Bader DA and McGuire SE: Tumour metabolism and its unique properties in prostate adenocarcinoma. Nat Rev Urol 17: 214-231, 2020.
4. Xing P, Wang S, Cao Y, Liu B, Zheng F, Guo W, Huang J, Zhao Z, Yang Z, Lin X, *et al*: Treatment strategies and drug resistance mechanisms in adenocarcinoma of different organs. Drug Resist Updat 71: 101002, 2023.
5. Rances OT and So JS: A rare case of prostatic malakoplakia associated with prostate adenocarcinoma: A case report and review of literature. Acta Med Indones 55: 339-342, 2023.
6. Yamada Y and Beltran H: Clinical and biological features of neuroendocrine prostate cancer. Curr Oncol Rep 23: 15, 2021.
7. Xie J, Tang Y, Wang Y, Gao X, Fu F, Liu Y, Yi C, Zhou G, Wang Z, Chen C, *et al*: Construction and verification of a prognostic model for prostate cancer based on ribosome Biogenesis-related genes. BMC Medical Genomics 18: 196, 2025.

8. Wang W, Zhang J, Wang Y, Xu Y and Zhang S: Identifies microtubule-binding protein CSPP1 as a novel cancer biomarker associated with ferroptosis and tumor microenvironment. Comput Struct Biotechnol J 20: 3322-3335, 2022.
9. Wang J, Wang Y, Zhou H, Yu G, Xu H, Gao D, Li M, Wang Y and Xu B: Identification of the specific characteristics of neuroendocrine prostate cancer: Immune status, hub genes and treatment. Transl Oncol 54: 102320, 2025.
10. Quan Y, Zhang H, Wang M and Ping H: UQCRB and LBH are correlated with Gleason score progression in prostate cancer: Spatial transcriptomics and experimental validation. Comput Struct Biotechnol J 23: 3315-3326, 2024.
11. Blando JM, Carbajal S, Abel E, Beltran L, Conti C, Fischer S and DiGiovanni J: Cooperation between Stat3 and Akt signaling leads to prostate tumor development in transgenic mice. Neoplasia 13: 254-265, 2011.
12. Huo SF, Shang WL, Yu M, Ren XP, Wen HX, Chai CY, Sun L, Hui K, Liu LH, Wei SH, *et al*: STEAP1 facilitates metastasis and epithelial-mesenchymal transition of lung adenocarcinoma via the JAK2/STAT3 signaling pathway. Biosci Rep 40: BSR20193169, 2020.
13. Kainov YA and Makeyev EV: A transcriptome-wide antitermination mechanism sustaining identity of embryonic stem cells. Nat Commun 11: 361, 2020.
14. Gamallat Y, Choudhry M, Li Q, Rokne JG, Alhajj R, Abdelsalam R, Ghosh S, Arbet J, Boutros PC and Bismar TA: Serrate RNA effector molecule (SRRT) is associated with prostate cancer progression and is a predictor of poor prognosis in lethal prostate cancer. Cancers (Basel) 15: 2867, 2023.
15. Yin J, Kim SS, Choi E, Oh YT, Lin W, Kim TH, Sa JK, Hong JH, Park SH, Kwon HJ, *et al*: ARS2/MAGL signaling in glioblastoma stem cells promotes self-renewal and M2-like polarization of tumor-associated macrophages. Nat Commun 11: 2978, 2020.
16. Luboldt W, Hartmann H, Wiedemann B, Zöphel K and Luboldt HJ: Gastroenteropancreatic neuroendocrine tumors: Standardizing therapy monitoring with 68Ga-DOTATOC PET/CT using the example of somatostatin receptor radionuclide therapy. Mol Imaging 9: 351-358, 2010.
17. Bemmo A, Dias C, Rose AA, Russo C, Siegel P and Majewski J: Exon-level transcriptome profiling in murine breast cancer reveals splicing changes specific to tumors with different metastatic abilities. PLoS One 5: e11981, 2010.
18. Nezamabadi Farahani L, Kazemnejad A, Afrasiabi M and Tapak L: Unlocking the potential of hybrid models for prognostic biomarker discovery in oral cancer survival analysis: A retrospective cohort study. Cell J 26: 688-699, 2025.
19. Wu T, Hu E, Xu S, Chen M, Guo P, Dai Z, Feng T, Zhou L, Tang W, Zhan L, *et al*: clusterProfiler 4.0: A universal enrichment tool for interpreting omics data. Innovation (Camb) 2: 100141, 2021.
20. Shi Y, Wang Y, Dong H, Niu K, Zhang W, Feng K, Yang R and Zhang Y: Crosstalk of ferroptosis regulators and tumor immunity in pancreatic adenocarcinoma: Novel perspective to mRNA vaccines and personalized immunotherapy. Apoptosis 28: 1423-1435, 2023.
21. Xu S, Hu E, Cai Y, Xie Z, Luo X, Zhan L, Tang W, Wang Q, Liu B, Wang R, *et al*: Using clusterProfiler to characterize multiomics data. Nat Protoc 19: 3292-3320, 2024.
22. Wissel D, Janakarajan N, Schulte J, Rowson D, Yuan X and Boeva V: sparsesurv: A Python package for fitting sparse survival models via knowledge distillation. Bioinformatics 40: btae521, 2024.
23. Sun Z, Hu M, Huang X, Song M, Chen X, Bei J, Lin Y and Chen S: Predictive value of dendritic cell-related genes for prognosis and immunotherapy response in lung adenocarcinoma. Cancer Cell Int 25: 13, 2025.
24. Ke AW, Shi GM, Zhou J, Huang XY, Shi YH, Ding ZB, Wang XY, Devbhandari RP and Fan J: CD151 amplifies signaling by integrin α6β1 to PI3K and induces the epithelial-mesenchymal transition in HCC cells. Gastroenterology 140: 1629-1641.e15, 2011.
25. Huang XY, Ke AW, Shi GM, Zhang X, Zhang C, Shi YH, Wang XY, Ding ZB, Xiao YS, Yan J, *et al*: αB-crystallin complexes with 14-3-3zeta to induce epithelial-mesenchymal transition and resistance to sorafenib in hepatocellular carcinoma. Hepatology 57: 2235-2247, 2013.
26. Wang J, Xiao Q, Chen X, Tong S, Sun J, Lv R, Wang S, Gou Y, Tan L, Xu J, *et al*: LanCL1 protects prostate cancer cells from oxidative stress via suppression of JNK pathway. Cell Death Dis 9: 197, 2018.
27. Dai DL, Martinka M and Li G: Prognostic significance of activated Akt expression in melanoma: A clinicopathologic study of 292 cases. J Clin Oncol 23: 1473-1482, 2005.
28. Ku SY, Wang Y, Garcia MM, Yamada Y, Mizuno K, Long MD, Rosario S, Chinnam M, Al Assaad M, Puca L, *et al*: Notch signaling suppresses neuroendocrine differentiation and alters the immune microenvironment in advanced prostate cancer. J Clin Invest 134: e175217, 2024.
29. Zaidi S, Park J, Chan JM, Roudier MP, Zhao JL, Gopalan A, Wadosky KM, Patel RA, Sayar E, Karthaus WR, *et al*: Single-cell analysis of treatment-resistant prostate cancer: Implications of cell state changes for cell surface antigen-targeted therapies. Proc Natl Acad Sci USA 121: e2322203121, 2024.
30. Nouruzi S, Johnson F, Kumar S, Sivak O, Tabrizian N, Koistinaho M, Muona A and Zoubeidi A: Targeting adenocarcinoma and enzalutamide-resistant prostate cancer using the novel anti-androgen inhibitor ADA-308. Oncol Rep 52: 132, 2024.
31. Zhuo X, Dai H and Yu S: The cGAS-STING pathway-related gene signature can predict patient prognosis and immunotherapy responses in prostate adenocarcinoma. Medicine (Baltimore) 101: e31290, 2022.
32. Nouruzi S, Namekawa T, Tabrizian N, Kobelev M, Sivak O, Scurll JM, Cui CJ, Ganguli D and Zoubeidi A: ASCL1 regulates and cooperates with FOXA2 to drive terminal neuroendocrine phenotype in prostate cancer. JCI Insight 9: e185952, 2024.
33. Hashemi M, Sabouni E, Rahmanian P, Entezari M, Mojtabavi M, Raei B, Zandieh MA, Behroozaghdam M, Mirzaei S, Hushmandi K, *et al*: Deciphering STAT3 signaling potential in hepatocellular carcinoma: Tumorigenesis, treatment resistance, and pharmacological significance. Cell Mol Biol Lett 28: 33, 2023.
34. Wu T, Wang W, Shi G, Hao M, Wang Y, Yao M, Huang Y, Du L, Zhang X, Ye D, *et al*: Targeting HIC1/TGF-β axis-shaped prostate cancer microenvironment restrains its progression. Cell Death Dis 13: 624, 2022.
35. Rodarte KE, Nir Heyman S, Guo L, Flores L, Savage TK, Villarreal J, Deng S, Xu L, Shah RB, Oliver TG and Johnson JE: Neuroendocrine differentiation in prostate cancer requires ASCL1. Cancer Res 84: 3522-3537, 2024.
36. Su Y, Liu Y, Behrens CR, Bidlingmaier S, Lee NK, Aggarwal R, Sherbenou DW, Burlingame AL, Hann BC, Simko JP, *et al*: Targeting CD46 for both adenocarcinoma and neuroendocrine prostate cancer. JCI Insight 3: e121497, 2018.
37. Kido LA, de Almeida Lamas C, Maróstica MR Jr and Cagnon VHA: Transgenic adenocarcinoma of the mouse prostate (TRAMP) model: A good alternative to study PCa progression and chemoprevention approaches. Life Sci 217: 141-147, 2019.
38. He Q, Huang Y, Cai L, Zhang S and Zhang C: Expression and prognostic value of Ars2 in hepatocellular carcinoma. Int J Clin Oncol 19: 880-888, 2014.
39. Luo J, Jiang B, Li C, Jia X and Shi D: CYC27 synthetic derivative of bromophenol from red Alga *Rhodomela confervoides*: Anti-diabetic effects of sensitizing insulin signaling pathways and modulating RNA Splicing-associated RBPs. Mar Drugs 17: 2019.